CrossMark

ORIGINAL PAPER

Effect of fragment size distribution on reaction rate and molecular weight distribution in heterogeneous olefin polymerization

Marzieh Nouri[1] · Mahmoud Parvazinia[1] · Hassan Arabi[1]

Abstract A one-dimensional polymeric flow model is used to study the effect of particle fragment size and size distribution on molecular weight distribution and particularly on reaction yield in heterogeneous olefin polymerization. The broadness of molecular weight distribution is explained by a multi-active site assumption, while the high rate of reaction for active catalysts due to diffusion limitations in the particle is questionable. In this study, the modeling is shifted from particle to fragment level. The fragments are assumed to be spherical and homogeneous with regular physical properties, separated from each other by interconnected cracks. There is only monomer diffusion taking place inside the particle, while in comparison the diffusion inside the cracks is much higher. Diffusion coefficient is assumed to be similar in all cracks. The polymer particle is taken to be made up of seven different size fragments from 0.5 to 3.5 μm, distributed in five different patterns. The results show that by introducing the fragments and fragment size distribution in the particle model higher yields of polymerization can be achieved. In other words, the fragments and cracks inside the particle can make strong impact on the reaction yield while the results show that the broadness of molecular weight and consequently a higher PDI can be justified by the multiple sites assumption.

✉ Mahmoud Parvazinia
   m.parvazinia@ippi.ac.ir

[1] Iran Polymer and Petrochemical Institute,
    P.O. Box: 14975/112, Tehran, Iran

Introduction

One of the most important routes for production of polyolefins (i.e., polyethylene, polypropylene and their copolymer with α-olefins) is accomplished by heterogeneous catalysts. In these processes, the reaction begins when small catalyst particles (20–100 μm in diameter) are injected into the reactor. The continuous phase of the reactor contains monomer(s) either in the form of gas or liquid which must diffuse through both the boundary layer around each catalyst particle and its pores to reach the active sites, where the polymerization takes place. The produced polymer deposits on the pores and the catalyst surface, then the monomer(s) must also diffuse through this polymer layer to reach the active sites. As the reaction proceeds, the catalyst particles grow to form a pseudo-homogeneous polymer particle with about 500–2500 μm in diameter. Typical heterogeneous catalysts currently used in polyolefin industry are single site silica-supported metallocene catalysts and multiple site MgCl$_2$/silica-supported Zeigler–Natta (ZN) catalysts.

A significant number of articles have been published to model the growth of catalyst particles in heterogeneous polymerization [1–3]. The two popular models most widely used in single particle modeling are the polymeric flow model (PFM) [4–6] and the multigrain model (MGM) [7–9]. Both models are considered to have reasonable approximations of the actual physical and chemical phenomena taking place in a polymer particle and can estimate the overall particle polymerization rate, particle temperature and molecular properties of the produced polymer. The PFM assumes that growing polymer chain and catalyst fragments form a continuum and the mass transfer in particle follows a Fickian diffusion mechanism through the pseudo-homogeneous polymer phase.

The MGM model provides a more detailed look into the growing polymer particle and considers the diffusion phenomena within micro- and macro-particle levels. With the extended versions of MGM, such as polymeric multigrain model (PMGM) [10, 11] and polymeric multilayer model (PMLM) [12–14], the former does neglect the diffusion resistance at the micro-particle level and the latter ignores the micro-particle to improve the initial MGM model. These models have shown success with low active catalyst. When the more active generations of heterogeneous catalyst emerged, the models failed to predict the high rate of polymerization. If the transport properties such as diffusion increases, then the broad molecular weight of the polymer cannot be justified by transport limitation and the multiple sites assumption can be used to justify the breath of molecular weight. While the molecular weight broadness can be modeled by multiple sites assumption, there is no justification for high rates of polymerization in the presence of transport limitation [1, 15]. To justify the high rates of polymerization, in some studies on single particle modeling, it is assumed that the mass transfer inside the particle occurs not only by diffusion, but also by the convection of the monomer through the particle. Therefore, some models were developed by introducing convective terms into the particle model [16–18].

Previously, some research groups focused on the modeling of the catalyst/polymer fragmentation and morphological development in olefin polymerization. Kittelsen et al. [19] introduced a viscoelastic model based on the magnitude and the generation rate of the mechanical stresses due to the produced polymer. Kosek et al. [20, 21] treated the polymer particle as an agglomeration of a large number of micro-elements and used a force balance between the neighboring micro-elements to predict the different morphology patterns of polyolefin particles. Recently, Parvazinia et al. [22–24] have introduced a two-dimensional PFM and considered the fragment patterns that affect the average molecular weight properties, the polymerization rate and the particle overheating in heterogeneous Ziegler–Natta olefin polymerization.

Machado et al. [25] have analyzed the very early development of particle morphology and polymer properties for three different Ziegler–Natta and supported metallocene commercial catalyst systems using stopped flow reactor. It is declared that, depending on the operating conditions, distinct non-uniform catalyst fragmentation patterns can develop. In addition, it is shown experimentally that the polydispersity of polymer at the initial moments of the polymerization is very high, suggesting the existence of significant concentration or temperature gradients. Although at very low degree of polymerization, multigrain structure is detected in SEM and TEM photographs of a nascent polymer [1, 26, 27], but micrograins merge into larger structures and form agglomerations when the reaction advances. These agglomerates would contain several fragments and could make larger structures in fully grown particles [28]. Cecchin et al. [29] have declared that a spherical particle of nascent polymer produced on $MgCl_2$/$TiCl_4$ catalyst comprises many polymer globules with diameter of around 1–2 μm and consists of microparticles which can be assimilated to the PFM. As well, the major portion of the porosity of the catalyst macro-particles is due to the spaces between sub-particles. According to this double grain morphology, they have named the whole system as a double grain model. Skomorokhov et al. [30] have for the first time used this name for their model, by assuming that polymer granules consist of some sub-particles with 10 % of the scale of the whole particle and each of them in turn consists of some microparticles having diameter of about 0.5 μm. It has been concluded that the size of sub-particles has a decisive effect on the yield of polymerization. Kittilsen et al. [31] have also proposed a three level model, micro- meso- and macro-level and included the fragments (meso-scale) in the model. The introduced meso-scale has about 10–40 % of the scale of the whole particle.

In this work, to justify the higher rates of polymerization in heterogeneous olefin polymerization, it is assumed that the particle consists of a number of fragments and in this respect the effect of fragment size and size distribution on the reaction rate, polymer yield and molecular weight distribution is studied. It is assumed that the catalyst particle is fully fragmented at the beginning of polymerization and no more fragmentation occurs during the reaction. This means that the number of fragments is taken to be constant, but the fragments are growing as polymerization proceeds. A polymeric flow model is used to model the growth of fragments and it is assumed that all fragments are spherical. The monomer concentration inside the cracks is assumed to be equal to monomer bulk concentration. Catalysts with single and double active sites are studied.

Table 1 Kinetic mechanism of heterogeneous catalytic olefin polymerization

Description	Reaction	Kinetic constant
Initiation	$C^{*k} + M \rightarrow P_1^k$	K_i^k
Propagation	$P_n^k + M \rightarrow P_{n+1}^k$	K_p^k
Transfer	$P_n^k \rightarrow C^{*k} + D_n^k$ $P_n^k + H \rightarrow C^{*k} + D_n^k$	K_{TR}^{k} [a]
Deactivation	$P_n^k \rightarrow C_d^k + D_n^k$ $C^{*k} \rightarrow C_d^k$	K_d^k

[a] $K_{TR}^k = K_{t\beta}^k + K_{tH}^k[H]$

Table 2 Net production–consumption rates of the leading moments of *living* and *dead* polymer chains

0th moment of *living* chains	$R_{\lambda_0^k} = K_i^k C^{*k} M - (K_{TR}^k + K_d^k)\lambda_0^k$
1st moment of *living* chains	$R_{\lambda_1^k} = K_i^k C^{*k} M - (K_{TR}^k + K_d^k)\lambda_1^k + K_p^k \lambda_0^k M$
2nd moment of *living* chains	$R_{\lambda_2^k} = K_i^k C^{*k} M - (K_{TR}^k + K_d^k)\lambda_2^k + K_p^k(\lambda_0^k + 2\lambda_1^k)M$
0th moment of *dead* chains	$R_{\mu_0^k} = (K_{TR}^k + K_d^k)\lambda_0^k$
1st moment of *dead* chains	$R_{\mu_1^k} = (K_{TR}^k + K_d^k)\lambda_1^k$
2nd moment of *dead* chains	$R_{\mu_2^k} = (K_{TR}^k + K_d^k)\lambda_2^k$
Monomer	$R_p = \sum\limits_{k=1}^{2}(K_p^k \lambda_0^k + K_i^k C^{*k})M$
Active site	$R_{C^{*k}} = -(K_d^k + K_i^k M)C^{*k} + K_{TR}^k \lambda_0^k$

Model development

Kinetic model

In the present study, the kinetic mechanism for olefin homopolymerization over heterogeneous catalysts includes chain initiation, propagation, site transformation and deactivation (Table 1). P_n^k and D_n^k are *living* and *dead* polymer chain of length n on kth type of active site, respectively. C^{*k} and C_d^k are the concentrations of *active* and *deactive* kth type of catalyst sites. It is assumed that the chain transfer to hydrogen forms the same site type C^{*k} and the rate constant for all steps is independent of the chain length [32]. Based on above kinetic mechanism, λ_i^k and μ_i^k are ith moments for *living* and *dead* polymer chains of the kth active site accordingly:

$$\lambda_i^k = \sum_{n=1}^{\infty} n^i P_n^k \tag{1}$$

$$\mu_i^k = \sum_{n=2}^{\infty} n^i D_n^k \tag{2}$$

The reaction rate equations of all molecular species are reported in Table 2. In Table 3, the numerical values of the kinetic rate constants of the heterogeneous catalytic systems are reported. These numerical values are in the range of commonly reported values in the literature [22, 33, 34].

Particle growth model

To predict the spatial evolution of monomer concentration and the polymerization rate in a single catalyst/polymer particle in olefin polymerization, the modified polymeric flow model [17] is used. The growing polymer particle and fragments are assumed to be spherical and pseudo-homogeneous with constant density. The particle is isothermal and there is no external boundary transfer resistance. The mass transport of monomer is by diffusion only and the mass transfer resistance of all the other species (Table 2) is assumed to be negligible. The monomer diffusion and

Table 3 Kinetic rate constants used for single-type-site and two-type-site catalysts [22, 33, 34]

Reaction constant	Two-type-site catalyst		Single-type-site catalyst	Dimension
	Site 1	Site 2		
K_i^k	3.52	1.76	2.64	m^3/(mol s)
K_p^k	3.52	1.76	2.64	m^3/(mol s)
K_{TR}^k	0.66	2.64	1.65	1/s
K_d^k	2×10^{-4}	2×10^{-4}	2×10^{-4}	1/s

consumption is included in the unsteady-state mass balances for growing polymer substructures.

The governing equation for the monomer concentration, M, in a growing polymer particle is described as follows:

$$\frac{\partial M}{\partial t} = \frac{1}{r}\frac{\partial}{\partial r}\left(D r^2 \frac{\partial M}{\partial r}\right) - R_{pf} \tag{3}$$

The boundary and initial conditions are:

$$M = M_{\text{bulk}} \quad r = R \tag{4}$$

$$\frac{\partial M}{\partial r} = 0 \quad r = 0 \tag{5}$$

$$R = R_0 \quad t = 0 \tag{6}$$

In which D, R_0 and M_{bulk} are the monomer diffusion coefficient, the radius of the initial catalyst/substructures and the monomer concentration, respectively. The system of governing differential equations is solved using the Runge–Kutta method.

Assuming that the all other molecular species in the growing polymer particle are not diffusion limited, the following dynamic conservation equation to describe the distribution of the molecular species ($X : C^{*k}$, λ_v^k and μ_v^k, $v = 0$, 1 and 2 and $k = 1, 2$) in the growing particle can be derived.

$$\frac{\partial X}{\partial t} = \frac{1}{r^2}\frac{\partial}{\partial r}\left(r^2 u X\right) + R_X \tag{7}$$

Table 4 Catalyst characteristics and physical and transport properties

	Description	Value	Dimension
D	Diffusion coefficient in fragments	10^{-11}–10^{-13}	m^2/s
M	Monomer concentration on fragment surfaces	2000	mol/m^3
ρ_c	Catalyst density	2840	kg/m^3
ρ_p	Polymer density	905	kg/m^3
C_0^*	Initial concentration of catalyst active site	0.05	mol/kg_{cat}
M_m	Molecular weight of monomer	0.042	kg mol
R_0	Initial catalyst radius	26×10^{-6}	m
R_{0f}	Initial fragment radius	0.5×10^{-6}–3.5×10^{-6}	m

The boundary and initial conditions are:

$$\frac{\partial X}{\partial r} = 0 \quad r = 0 \tag{8}$$

$$X = X_0 \quad t = 0 \tag{9}$$

where R_X is the net production/consumption rate of species X (Table 2). At time zero, the concentrations of $\lambda_{v,0}^k$ and $\mu_{v,0}^k$ are equal to zero, while the concentration of the catalyst active sites at time $t = 0$, C_0^{*k} is equal to a selected value (Table 4).

Due to the polymer formation, the initial catalyst particle volume will grow with time. Assuming that the polymer phase behaves as an incompressible medium, the following pseudo-steady state mass conservation equation is derived to describe the particle volume change with time:

$$4/3\pi r^2 \frac{dr}{dt} = 4\pi \int_0^r \frac{M_m R_p}{\rho_p} r^2 dr \tag{10}$$

where $\frac{dr}{dt} = u$ (in $m^3/(s\,m)$) denotes the flux volumetric flow rate of the growing polymer phase.

Equations (1)–(10) are used to calculate the monomer and other species concentrations for each catalyst fragment.
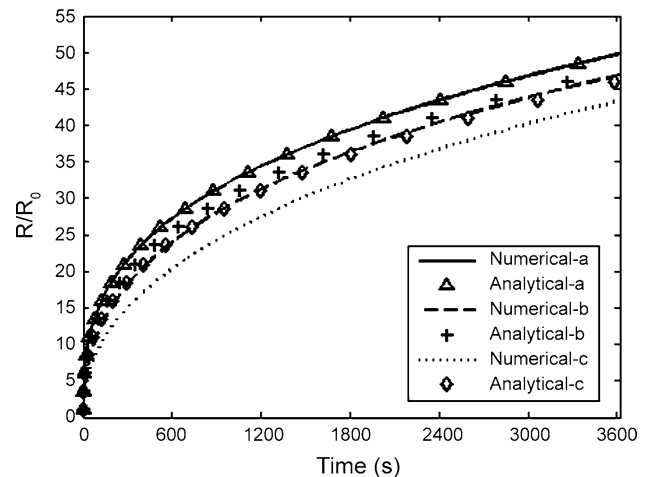
For each fragment, to calculate the number and the weight average chain lengths ($\overline{X}_{nf}$ and $\overline{X}_{wf}$) of the polymer chains produced over the two-type-site catalyst, the following equations are employed:

$$\overline{X}_{nf} = \frac{\sum_{k=1}^2 \left(\lambda_1^k + \mu_1^k \right)}{\sum_{k=1}^2 \left(\lambda_0^k + \mu_0^k \right)} \tag{11}$$

$$\overline{X}_{wf} = \frac{\sum_{k=1}^2 \left(\lambda_2^k + \mu_2^k \right)}{\sum_{k=1}^2 \left(\lambda_1^k + \mu_1^k \right)} \tag{12}$$

To calculate the polymerization rate of whole particle at any moment, the following equation is used:

$$R_P = \sum_{i=1}^m w_i R_{pf_i} \tag{13}$$

Fig. 1 Comparison of analytical and numerical results of particle growth. (a) $\theta = \sqrt{9.4}$, (b) $\theta = \sqrt{85}$ and (c) $\theta = \sqrt{150}$
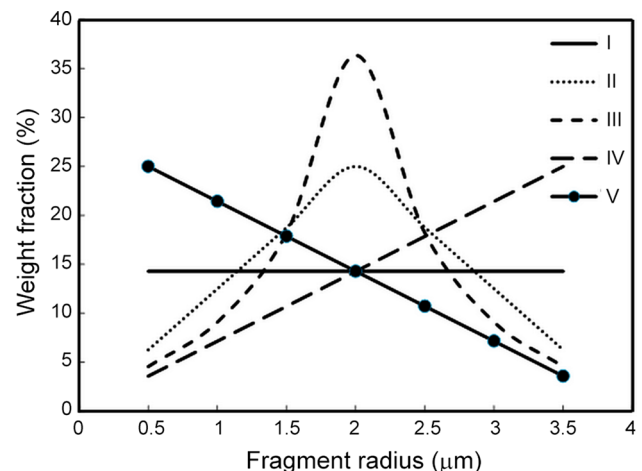
Fig. 2 Different fragment size distribution of a non-uniform fragmented catalyst

where m is the total number of fragments in the particle and w is the weight fraction of the polymer produced by fragment i at a time.

Equations (14) and (15) are used to calculate the number and the weight average chain lengths of whole particle, respectively.

$$\overline{X}_n = \frac{\sum_{i=1}^{m} W_i}{\sum_{i=1}^{m}\left(\frac{W_i}{\overline{X}_{nf_i}}\right)} \tag{14}$$

$$\overline{X}_w = \frac{\sum_{i=1}^{m} \overline{X}_{nf_i} W_i}{\sum_{i=1}^{m} W_i} \tag{15}$$

Model validation

To assess the accuracy of the numerical approach, simulation results can be compared with the results obtained from the approximated analytical solution. If we assume a pseudo-steady-state approximation for the monomer concentration in the growing polymer particle and also assuming that the "living" polymer chains and catalyst active sites are uniformly distributed in a growing particle, Eq. (3) can be written as follows:

Scheme 1 Schematic picture of a non-uniform fragmented catalyst

Scheme 2 Schematic picture of a uniform fragmented catalyst

$$0 = \frac{1}{r}\frac{\partial}{\partial r}\left(Dr^2\frac{\partial M}{\partial r}\right) - K_p M C_t^* \tag{16}$$

where C_t^* (in mol/m^3) denotes the total concentration of "living" polymer chains and catalyst active sites in the particle. The solution to Eq. (16) is given by Kosek et al. [20]:
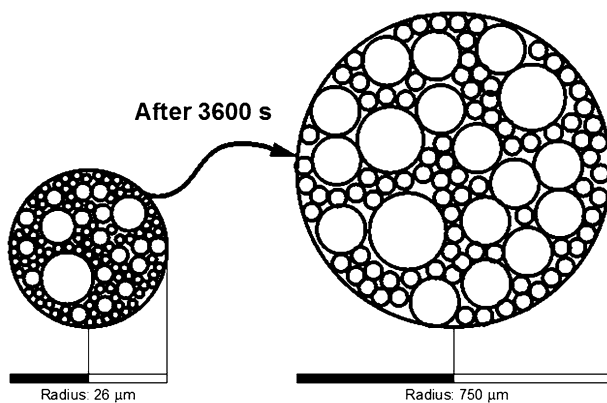
$$\frac{M(r,t)}{M} = \frac{R_t}{r}\frac{\sin h(\theta r/R_t)}{\sin h(\theta)} \tag{17}$$

where R_t is the particle radius at time t and θ, the Thiele modulus is equal to:
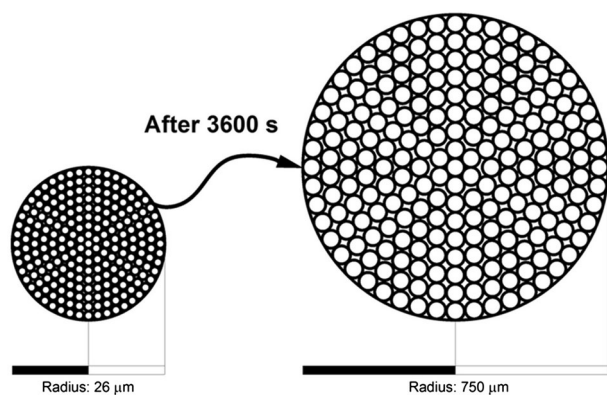
$$\theta = \sqrt{R_t^2 K_p C_t^*\Big/ D} \tag{18}$$

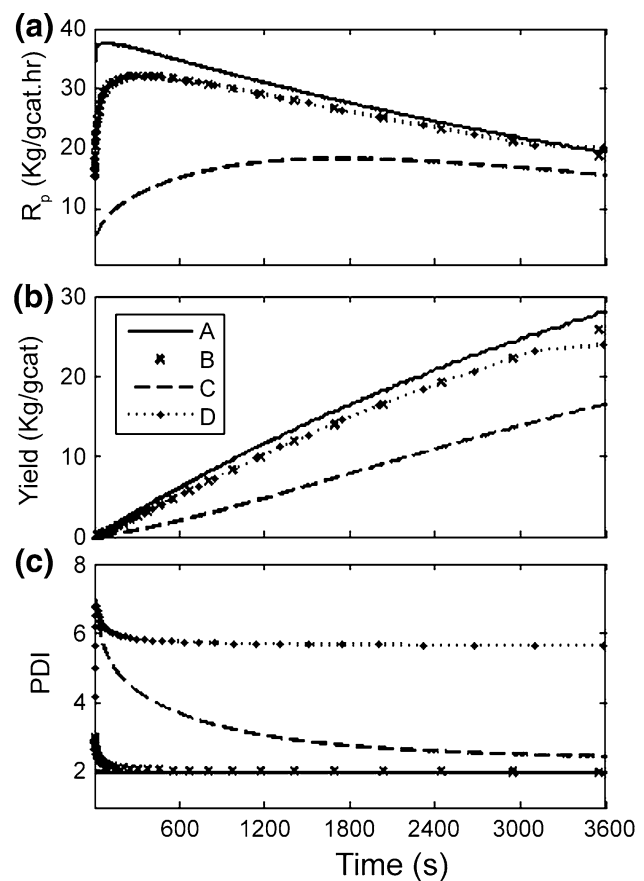θ_0 is the Thiele modulus value at time $t = 0$, defined by:

$$\theta_0 = \sqrt{R_0^2 K_p C_0^*\Big/ D} \tag{19}$$

Fig. 3 Dynamic evolution of the R_p (**a**) yield (**b**) and PDI (**c**) for a uniform fragmented catalyst. (*A*), (*B*) and (*C*) correspond to a single-type-site catalyst with $D = 1 \times 10^{-11}$ (m^2/s), $D = 2 \times 10^{-12}$ (m^2/s) and $D = 5 \times 10^{-13}$ (m^2/s), respectively. *D* corresponds to a two-type-site catalyst with $D = 2 \times 10^{-12}$ (m^2/s)

where C_0^* denotes the initial concentration of catalyst active sites in the particle and R_0 is the radius of the initial catalyst/substructures.

The time-varying particle radius, R_t, depends on the overall particle polymerization rate and is given by:

$$R_t^2 \frac{dR_t}{dt} = \int_0^{R_t} \frac{K_p C_t^* M(r,t) M_m}{\rho_p} r^2 dr \qquad (20)$$

By substituting Eq. (17) into Eq. (20) and integrating the resulting equation, R_t as function of time is obtained as follows:

$$\int_{R_0}^{R_t} \frac{R_t^2 dr}{\left(\frac{\cot h(\theta)}{\theta} - \frac{1}{\theta^2}\right)} = \frac{K_p C_0^* M M_m R_0^3}{\rho_p} t \qquad (21)$$

In Fig. 1, simulation results obtained from the numerical solution are compared with the analytical solution for three

different values of Thiele modulus. In the analytical solution $K_p = 2.64$ (m³/(mol s)), $K_d = 0$ (1/s) and other properties are listed in Table 4. As Fig. 1 shows, in the absence of monomer diffusion limitations (i.e., for low values of the Thiele modulus $\theta = \sqrt{9.4}$), the agreement between the approximate analytical solution and the numerical results is obtained. However, when the system is diffusion limited, the assumption of analytical solution is not true anymore and the analytical solution overestimates the rate of particle growth.

Result and discussion

In this study, the growth evolution of a fragmented catalyst particle is modeled to investigate the effect of fragment size distribution and the mass transfer resistance on the molecular weight distribution and particularly on the
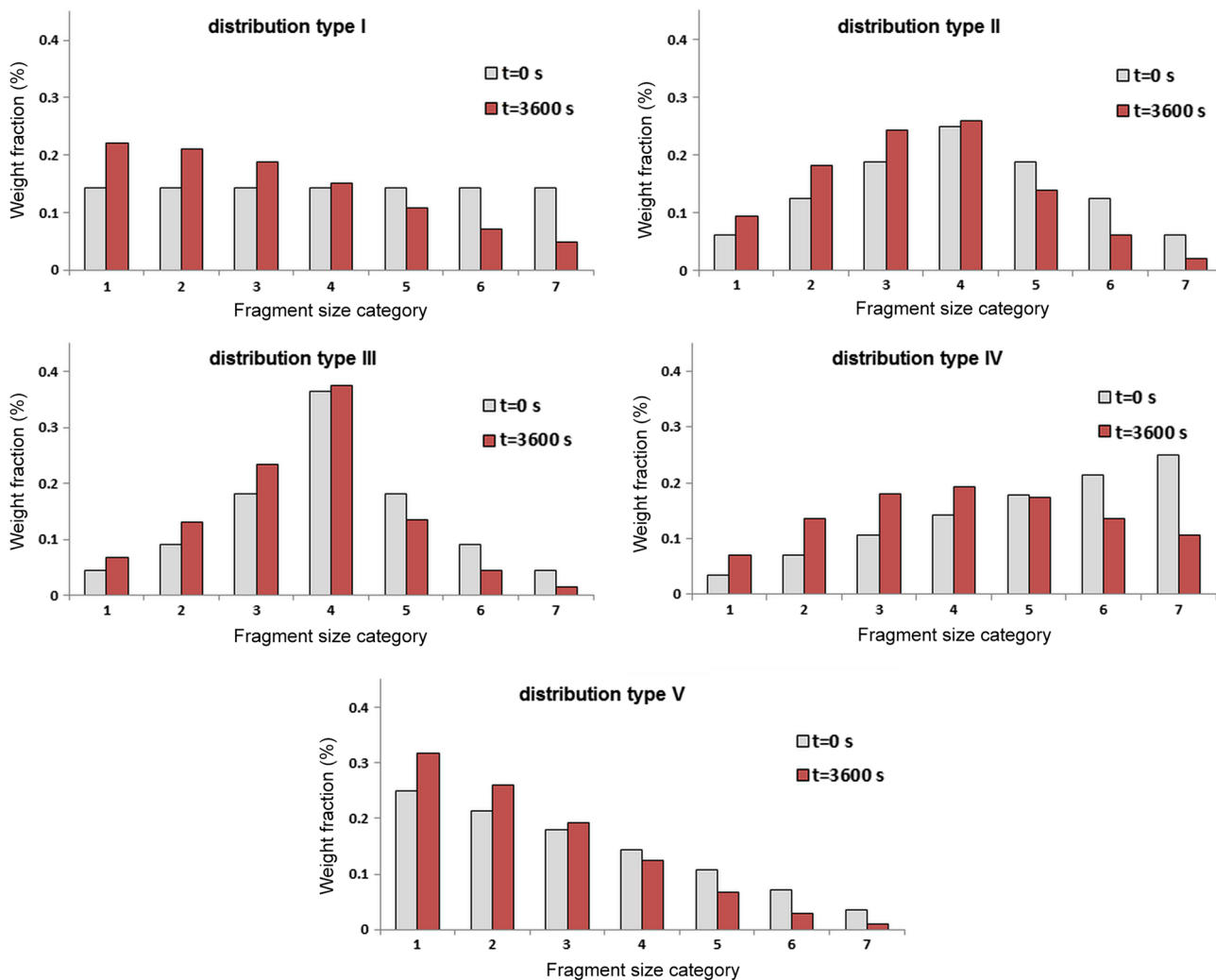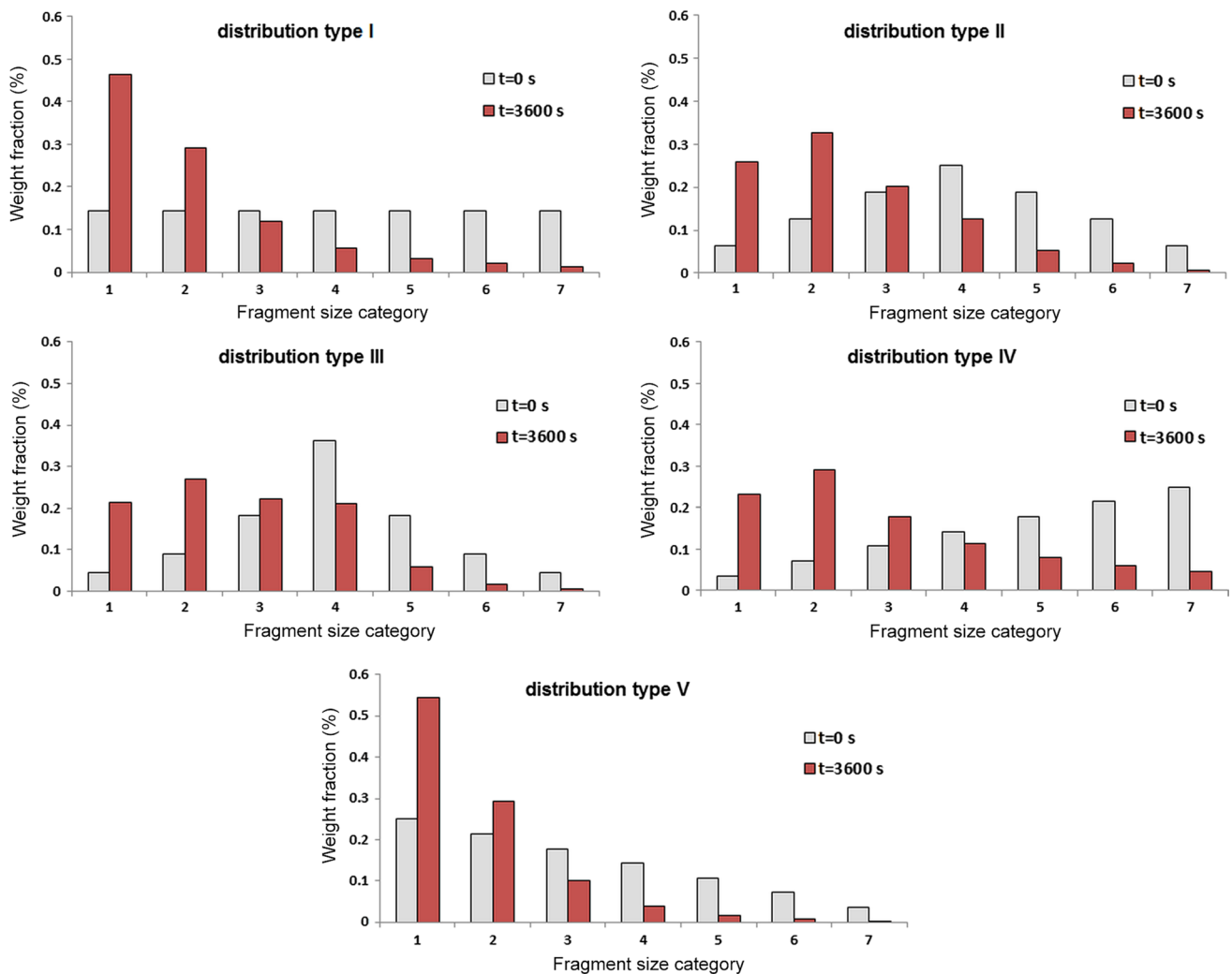

Fig. 4 Fragment size distribution in $t = 0$ s and $t = 3600$ s of polymerization time if $D = 1 \times 10^{-11}$ (m²/s)

reaction rate and yield of polymerization. The broadness of molecular weight distribution is explained by multi-active site assumption, while the high rate of polymerization for active catalysts is still a question. It is assumed that the polymer particle is made up of seven different size fragments from 0.5 to 3.5 μm and the number of fragments is constant, but they grow in the course of polymerization. The fragments are separated from each other by interconnected cracks, and the monomer concentration inside the cracks is assumed to be equal to the bulk concentration. PFM is used to model the polymerization process inside the fragments and in fragment level the polymerization is diffusion controlled. The effect of intraparticle mass transfer will be the most pronounced in a semi-crystalline polymer, while the polymer surrounding the active sites becomes thicker and the diffusion

coefficient in the dense polymer zone in the particle is about 10^{-12} (m^2/s) [8, 9, 11].

Five different fragment size distributions of a non-uniform fragmented catalyst based on the weight fractions used in this study are shown in Fig. 2 and each contains seven different size fragments from 0.5 to 3.5 μm. Scheme 1 shows the schematic picture of a non-uniform fragmented catalyst and the fragment size distributions in the polymer particle after 3600 s of polymerization time. The schematic picture of a uniform fragmented catalyst, in which the initial radius of all fragments is 0.5 μm, is illustrated in Scheme 2 and the polymer particle after 3600 s of polymerization time is still uniformly fragmented.

Figure 3 presents the dynamic evolution of the rate of polymerization, yield and PDI for a uniform fragmented

Fig. 5 Fragment size distribution in $t = 0$ s and $t = 3600$ s of polymerization time if $D = 2 \times 10^{-12}$ (m^2/s)
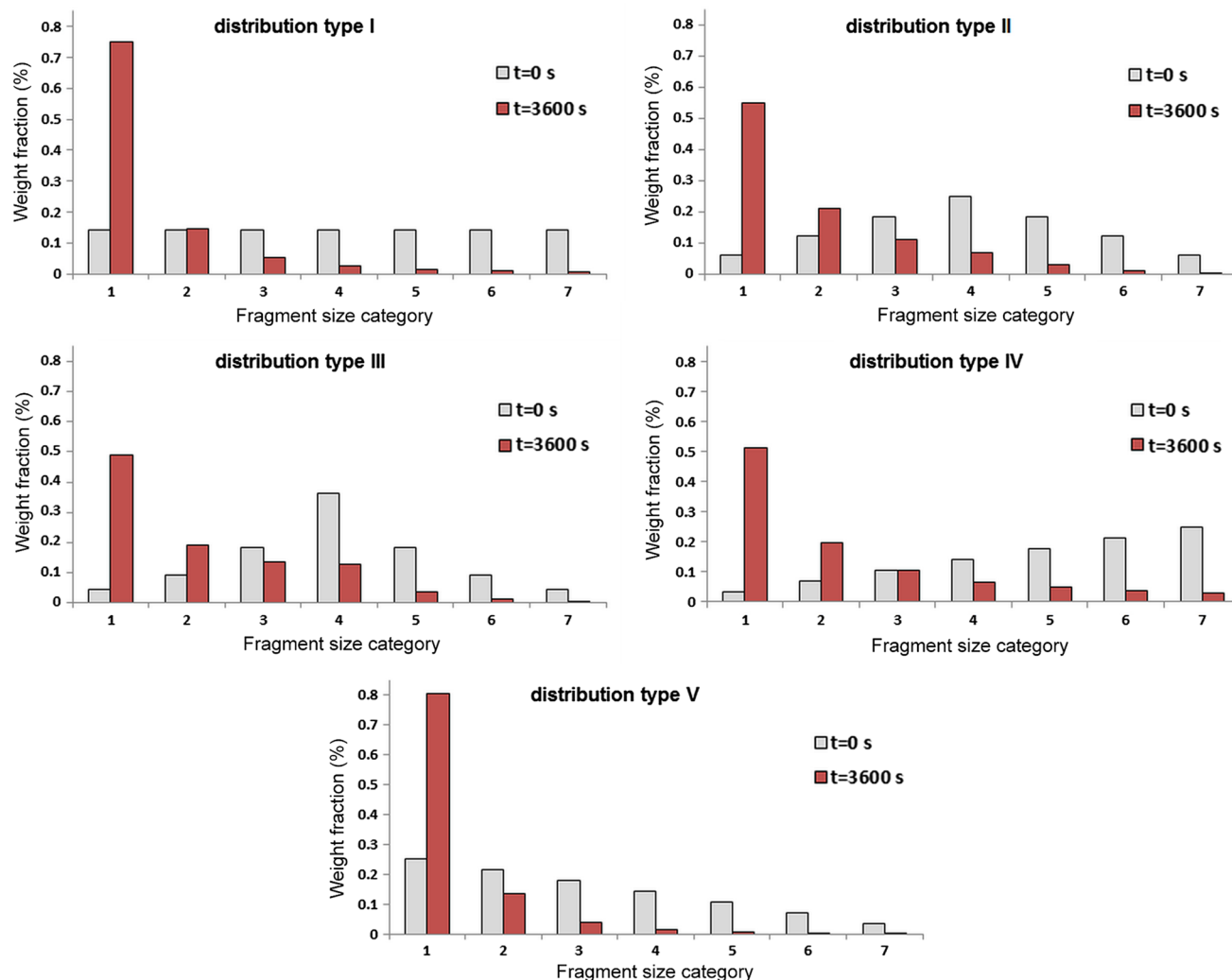
Fig. 6 Fragment size distribution in $t = 0$ s and $t = 3600$ s of polymerization time if $D = 5 \times 10^{-13}$ (m²/s)

catalyst with three different monomer diffusion coefficients. It can be seen that using a two-site kinetic assumption (curves D) while the yield is nearly the same, the PDI would be considerably higher. The inclusion of fragments generates a higher reaction rate and yield, while a two-site assumption generates a higher molecular weight distribution.

For non-uniform fragmented catalysts, Figs. 4, 5 and 6 show the weight fractions of different fragment size categories at the first moment of the reaction and after 3600 s of the polymerization time for three different monomer diffusion coefficients of 1×10^{-11}, 2×10^{-12} and 5×10^{-13} m²/s, respectively. All cases show that the smaller fragments grow faster and the weight fractions of the fragments with larger initial sizes are found to be larger; but it does not mean that they are larger than the fragments with a larger initial size. For example, when the

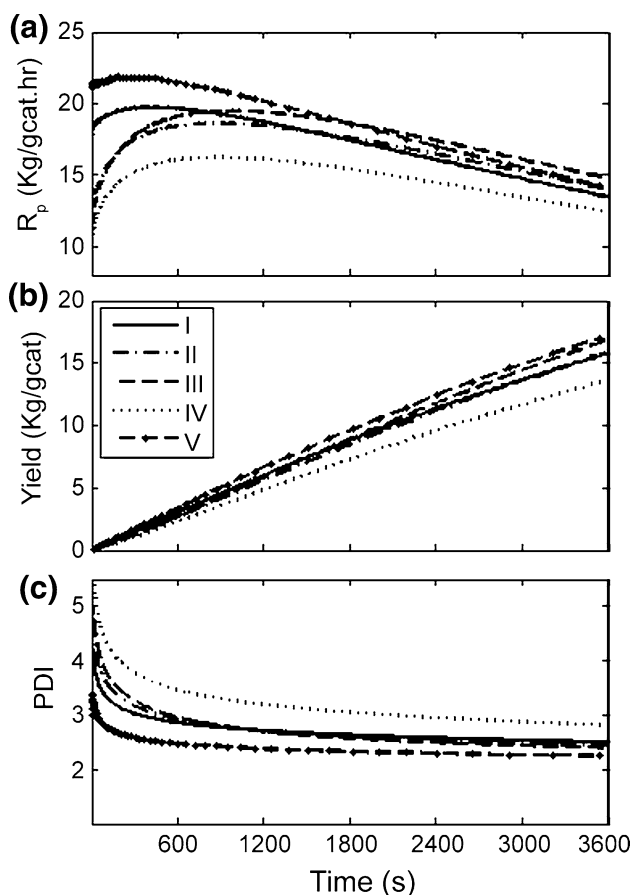**Table 5** Initial radiuses and final radiuses for each fragment size

Fragment size category	R_{0f} (µm)	R_f (µm) after 3600 s		
		$D = 1 \times 10^{-11}$	$D = 2 \times 10^{-12}$	$D = 5 \times 10^{-13}$
1	0.5	22.3	21.8	18.7
2	1	43.7	37.3	21.6
3	1.5	63.1	41.6	22.9
4	2	78.5	43.2	23.9
5	2.5	87.5	44.5	24.9
6	3	91.3	45.7	25.8
7	3.5	93.3	46.9	26.6

diffusion coefficient inside the fragments is 1×10^{-11} m²/s, the weight fraction of the first fragment size category in the distribution type 1 is increased from 14.7 wt% to

about 22 wt%. By decreasing the diffusion coefficient to 5×10^{-13} m²/s, the fragments with smaller initial size grow even faster and their weight fractions are found to be larger (about 75 wt%). The exact value of the initial radius (R_{0f}) and the radius after 3600 s (R_f) of polymerization time for each fragment size category in the three different diffusion are reported in Table 5. Fragment size distribution in a growing particle is strongly affected by mass transfer resistance. By increasing the mass transfer resistance, the impact of initial fragment size distribution is reduced. For instance, if the diffusion coefficient inside the fragments set is 5×10^{-13} m²/s (Fig. 6), then after 3600 s, the fragment size distribution is nearly identical for all initial distributions.

The reaction rate, polymer yield and PDI of different fragment size distributions in the single-type-site catalyst with 1×10^{-11} m²/s monomer diffusion are shown in Fig. 7. Larger weight fractions of the smaller fragments (case V) result in an increase in the yield and reaction rate but the weight fractions of larger fragments show no significant effect on the reaction rate and polymer yield (cases

III and IV). As the weight fraction of the smaller fragments increases, the PDI decreases accordingly. In smaller fragments, the monomer concentration gradient decreases and it is the main reason for the reduction in PDI. It is generally accepted that, the PDI of the polymer produced by single-type-site catalyst is about 2 when there is no mass transfer resistance [32].

In all cases of different fragment size distributions, by reducing the monomer diffusivity to 2×10^{-12} m²/s, the yield decreases and the PDI increases accordingly (Fig. 8). These observations are consistent with the results of uniform fragmented catalysts illustrated in Fig. 3. In cases I and V where the weight fractions of the smaller fragments are higher, the polymerization rate and yield, in the higher rates (for instance Fig. 8) take a considerable distance from the other cases. By further decreasing to 5×10^{-13} m²/s (Fig. 9), the differences between the two cases of I and V become even smaller.

The main objective of this work is to study the effect of fragment size distribution on polymer yield and molecular weight. Since the multiple sites assumption
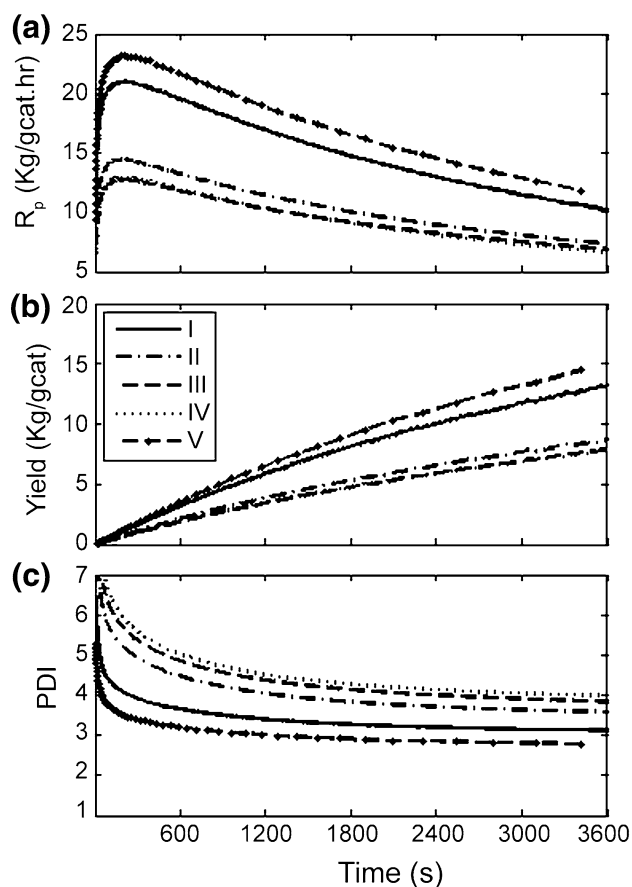
Fig. 7 Dynamic evolution of the R_p (**a**), yield (**b**) and PDI (**c**) for different fragment size distribution of a single-type-site catalyst with $D = 1 \times 10^{-11}$ (m²/s)

Fig. 8 Dynamic evolution of the R_p (**a**), yield (**b**) and PDI (**c**) for different fragment size distribution of a single-type-site catalyst with $D = 2 \times 10^{-12}$ (m²/s)

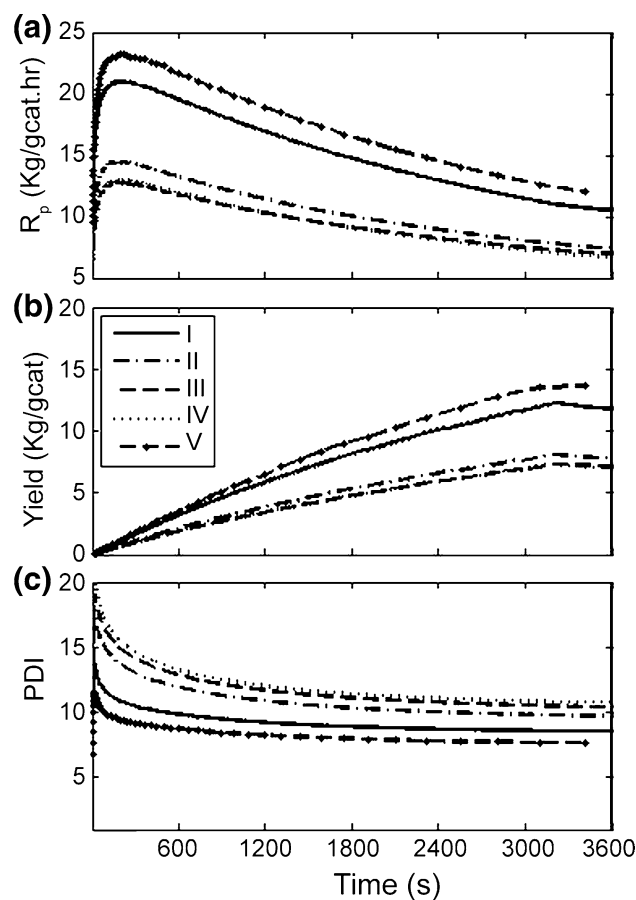Iran Polymer and Petrochemical Institute   Springer
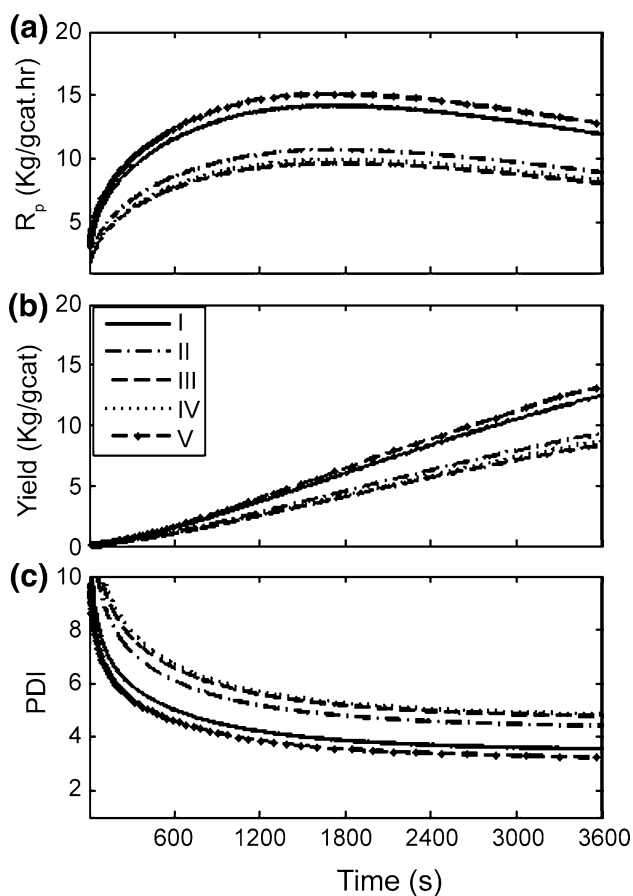
Fig. 9 Dynamic evolution of the R_p (**a**), yield (**b**) and PDI (**c**) for different fragment size distribution of a single-type-site catalyst with $D = 5 \times 10^{-13}$ (m²/s)

Fig. 10 Dynamic evolution of the R_p (**a**), yield (**b**) and PDI (**c**) for different fragment size distribution of two-type-site catalyst with $D = 2 \times 10^{-12}$ (m²/s)

is widely accepted to justify the broadness of molecular weight distribution, the catalyst with two-type active sites is studied. The same concentration of active sites and mean propagation rate for the single-type-site catalyst are considered (Table 3). As can be seen in Fig. 10, the reaction rate and polymer yield display the same trend as is usual in a single-type-site catalyst. According to Fig. 10, by applying the multiple sites assumption, the PDI can also be increased while there are a relatively high rate and yield as mentioned before in discussing Fig. 3.

Finally, for comparison with a normal PFM model of a single particle with no fragmentation, the reaction rate, polymer yield and PDI of the non-fragmented single-type-site catalyst with 1×10^{-11} and 2×10^{-12} m²/s monomer diffusion are represented in Fig. 11. As it can be seen, the yield is very low, but the PDI is higher than the fragmented cases. It shows that the fragments play an essential role in reaction yield while PDI can mainly be generated by a multiple sites assumption.

Conclusion

In this paper, the modeling of a single particle heterogeneous catalyst at fragment level (sub-particle level) is carried out and the effect of fragment size and size distribution on the reaction rate, polymer yield and polydispersity index is examined. It was assumed that the catalyst particle is fully fragmented in different fragment sizes and different fragment size distributions at the beginning of polymerization and the number of fragments was taken to be constant, but the fragments were grown based on the polymeric flow model assumptions as polymerization proceeded. The interconnected cracks separated fragments and the monomer concentration at the surface of fragments was assumed to be equal to the bulk concentration. The main purpose of the research was to justify the high rates of polymerization in spite of diffusional limitations. As the results show, by introducing fragment size and size distribution in the particle model, much higher yields of polymerization could be achieved. The results indicate that the smaller fragments
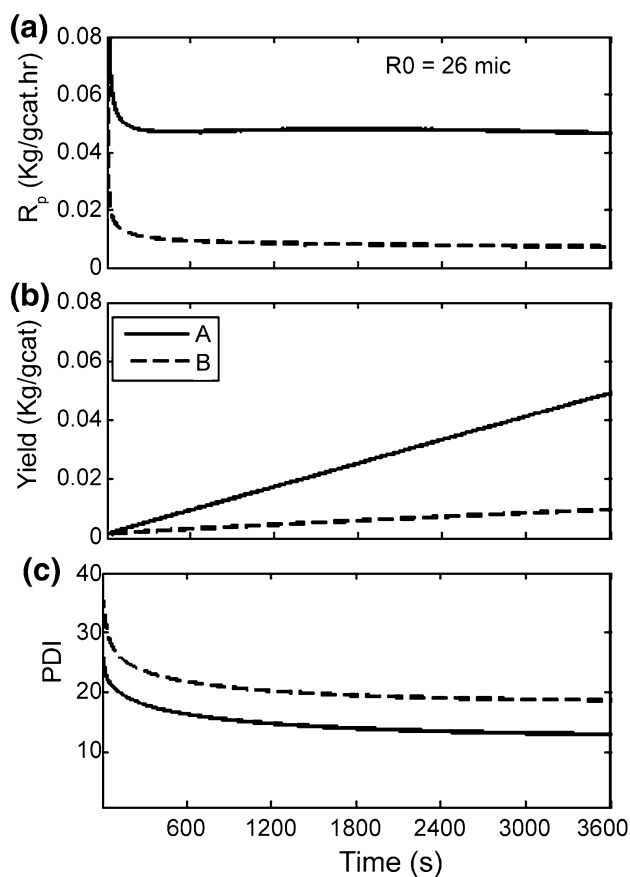
Fig. 11 Dynamic evolution of the R_p (**a**), yield (**b**) and PDI (**c**) for a non-fragmented single-type-site catalyst. (*A*) and (*B*), respectively, correspond to $D = 1 \times 10^{-11}$ (m²/s) and $D = 2 \times 10^{-12}$ (m²/s)

inside the particle make a strong impact on the increase of reaction yield.

References

1. McKenna TF, Soares JBP (2001) Single particle modelling for olefin polymerization on supported catalysts: a review and proposals for future developments. Chem Eng Sci 56:3931–3949

2. Dube MA, Soares JBP, Penlidis A, Hamielec AE (1997) Mathematical modelling of multicomponent chain-growth polymerizations in batch, semi-batch, and continuous reactors: a review. Ind Eng Chem Res 36:966–1015

3. Mattos Neto AG, Pinto JC (2001) Steady state modeling of slurry and bulk propylene polymerizations. Chem Eng Sci 56:4043–4057

4. Schmeal WR, Street JR (1971) Polymerization in expanding catalyst particles. AIChE J 17:1188–1197

5. Singh D, Merrill RP (1971) Molecular weight distribution of polyethylene produced by Ziegler–Natta catalysts. Macromolecules 4:599–604

6. Kanellopoulos V, Dompazis G, Gustafsson B, Kiparissides C (2004) Comprehensive analysis of single-particle growth in heterogeneous olefin polymerization: the random-pore polymeric flow model. Ind Eng Chem Res 43:5166–5180

7. Nagel EJ, Klrillov VA, Ray WH (1980) Prediction of molecular weight distributions for high-density polyolefins. Ind Eng Chem Prod Res Dev 19:372–379

8. Floyd S, Choi KY, Taylor TW, Ray WH (1986) Polymerization of olefins through heterogeneous catalysis. III. Polymer particle modelling with an analysis of intraparticle heat and mass transfer effects. J Appl Polym Sci 32:2935–2960

9. Hutchinson RA, Chen CM, Ray WH (1992) Polymerization of olefins through heterogeneous catalysts X: modelling of particle growth and morphology. J Appl Polym Sci 44:1389–1414

10. Sarkar P, Gupta SK (1991) Modelling of propylene polymerization in an isothermal slurry reactor. Polymer 32:2842–2852

11. Chen Y, Liu X (2005) Modeling mass transport of propylene polymerization on Ziegler–Natta catalyst. Polymer 46:9434–9442

12. Soares JBP, Hamielec AE (1995) General dynamic mathematical modeling of heterogeneous Ziegler-Natta and metallocene catalyzed copolymerization with multiple site types and mass and heat transfer resistances. Polym React Eng 3:261–324

13. Sun JZ, Eberstein C, Reichert KH (1997) Particle growth modeling of gas phase polymerization of butadiene. J Appl Polym Sci 64:203–212

14. Wang W, Zheng ZW, Luo ZH (2011) Coupled single-particle and Monte Carlo model for propylene polymerization. J Appl Polym Sci 119:352–362

15. Galvan R, Tirrell M (1986) Molecular weight distribution predictions for heterogeneous Ziegler–Natta polymerization using a two-site model. Chem Eng Sci 41:2385–2393

16. Veera UP, Weickert G, Agarwal US (2002) Modeling monomer transport by convection during olefin polymerization. AIChE J 48:1062–1070

17. Kittilsen P, Svendsen H, McKenna TF (2001) Modeling of transfer phenomena on heterogeneous Ziegler–Natta catalyst. IV. Convection effects in gas phase processes. Chem Eng Sci 56:3997–4005

18. Liu X (2007) Modeling and simulation of heterogeneous catalyzed propylene polymerization. Chin J Chem Eng 15:545–553

19. Kittilsen P, Svendsen HF, McKenna TF (2003) Viscoelastic model for particle fragmentation in olefin polymerization. AIChE J 49:1495–1507

20. Grof Z, Kosek J, Marek M (2005) Modeling of morphogenesis of growing polyolefin particles. AIChE J 51:2048–2067

21. Horackova B, Grof Z, Kosek J (2007) Dynamics of fragmentation of catalyst carriers in catalytic polymerization of olefins. Chem Eng Sci 62:5264–5270

22. Najafi M, Parvazinia M, Ghoreishy MHR, Kiparissides C (2014) Development of a two dimensional finite element isothermal particle model to analyze the effect of initial particle shape and breakage in olefin polymerization. Macromol React Eng 8:29–45

23. Najafi M, Parvazinia M, Ghoreishy MHR (2014) Modelling the catalyst fragmentation pattern in relation to molecular properties and particle overheating in olefin polymerization. Polyolefin J 1:77–91

24. Najafi M, Parvazinia M (2015) Computational modeling of particle fragmentation in the heterogeneous olefin polymerization. Macromol Theory Simul 24:28–40

25. Machado F, Lima EL, Pinto JC, McKenna TF (2011) An experimental study on the early stages of gas-phase olefin polymerizations using supported Ziegler–Natta and metallocene catalysts. Polym Eng Sci 51:302–310

26. Kakugo M, Sadatoshi H, Sakai J, Yokoyama M (1989) Growth of polypropylene particles in heterogeneous Ziegler–Natta polymerization. Macromolecules 22:3172–3177

27. McKenna TF, Di Martino A, Weickert G, Soares JBP (2010) Particle growth during the polymerisation of olefins on supported catalysts, 1—nascent polymer structures. Macromol React Eng 4:40–64

28. Martin Ch, McKenna TF (2002) Particle morphology and transport phenomena in olefin polymerization. Chem Eng J 87:89–99

29. Cecchin G, Marchetti E, Baruzzi G (2001) On the mechanism of propylene growth over $MgCl_2/TiCl_4$ catalyst systems. Macromol Chem Phys 202:1987–1994

30. Skomorokhov VB, Zakharov VA, Kirillov VA, Bukatov GD (1989) Mass transfer in polymerization of olefins on solid catalysts. The double-grain model. Polym Sci USSR 31:1420–1429

31. Kittilsen P, Svendsen HF (2004) Three-level mass-transfer model for the heterogeneous polymerization of olefins. J Appl Polym Sci 91:2158–2167

32. Soares JBP, McKenna T, Cheng CP (2007) In: Asua JM (ed) Polymer reaction engineering, 1st edn. Blackwell, UK

33. Bukatov GD, Zakharov VA (2001) Propylene Ziegler–Natta polymerization: numbers and propagation rate constants for stereospecific and non-stereospecific centers. Macromol Chem Phys 202:2003–2009

34. Taniike T, Nguyen BT, Takahashi S, Vu TQ, Ikeya M, Terano M (2011) Kinetic elucidation of comonomer-induced chemical and physical activation in heterogeneous Ziegler–Natta propylene polymerization. J Polym Sci Part A Polym Chem 49:4005–4012